Materials Research Proceedings 54 (2025) 478-486 https://doi.org/10.21741/9781644903599-52

Investigating the strength of adhesively bonded SMC components

Michele Tropeano[1,a], Gianluca Gatti[1,b], Luca Raimondi[1,c], Lorenzo Donati[1,d], Davide Serradimigni[2,e]

[1]Viale del Risorgimento, 2, 40136 Bologna (BO), Italy

[2]Via del Tirassegno, 55, 41122 Modena (MO), Italy

[a]michele.tropeano2@unibo.it, [b]gianluca.gatti7@unibo.it, [c]luca.raimondi@unibo.it, [d]l.donati@unibo.it, [e]d.serradimigni@cpcgroup.it

Keywords: Sheet Molding Compound, Adhesives, Composite Joining

Abstract. Sheet Molding Compound (SMC) has emerged as a compelling alternative to light metal alloys to produce lightweight structural components in several industries. Despite their advantages, the complexity introduced by random short-fiber reinforcement SMC materials makes their mechanical behavior challenging to predict using Finite Element Analysis (FEA) models. These challenges extend to evaluating and predicting the bonding strength of adhesive joints involving such materials, which is critical in many automotive and aerospace applications. This research proposes a methodology for generating accurate material cards for adhesives/joints. The approach integrates experimental testing, numerical modeling, and optimization. A three-phase process was employed, utilizing software such as HyperMesh, Abaqus, and HyperStudy. The optimization phase involved the Design of Experiments (DOE) to explore parameter spaces, fitting to construct response surfaces, and optimization algorithms to refine material properties for curve matching. Despite the challenges posed by the brittle nature of SMC substrates, the approach successfully captured the joint's mechanical behavior, producing a reliable material card for this specific material combination. This study underscores the potential of the proposed methodology to predict joint strength in large-scale simulations, such as full-vehicle assemblies, with improved accuracy and reliability. By addressing the unique challenges of SMC materials, this work provides a robust framework for adhesive characterization and enhances structural designs in composite bonding applications.

Introduction

In the past two decades, polymeric composite materials have garnered significant attention across various industries due to their exceptional properties, including modulus, strength, and energy absorption [1–3]. The automotive sector, in particular, serves as a leading example of innovation in the application of these materials [4]. Among different methods, the sheet molding compound (SMC) process stands out as the top choice for producing composite structures in the automotive sector, primarily because of its impressive ability to facilitate high-volume production [5]. In industrial applications, the joining of SMC components is currently performed in several ways, each with specific limitations. The use of bolts [6], rivets, and inserts [7,8] is a common practice to connect SMC structures to other components. Nonetheless, these joints may add significant weight to the overall structure, are prone to galvanic corrosion [9], and often require a more complex mold design to embed them successfully. Another conventional solution for joining this material is adhesive bonding. The main limitation of the widespread use of this technology in joining SMC material is a lack of understanding of fracture mechanisms [10]. Jyoti and coworkers [11] examined the Mode I fracture toughness of SMC materials, analyzing samples with and without an adhesive layer. In the specimens bonded with adhesive, the cracks developed either along the interface between the composite and adhesive or within the composite material itself.

Several research highlighted the difficulties in characterizing Mode II fracture toughness of automotive class adhesive bonded joints with SMC adherend [12,13]. It can be argued that the lack of well-established characterization strategies hinders the use of Finite Element Analysis (FEA) to numerically study the behavior of SMC adhesively bonded joints. This implies the need to fabricate bonded components and experimentally investigate if they will have the desired functionalities through expensive experimental tests. In this work, the possibility of predicting the strength of adhesively bonded SMC components by means of numerical tools is investigated. Several SMC plates were compression molded and cut to extract the adherends for subsequent bonding. Two specifically designed jigs were used to position the specimens and to calibrate the thickness of the adhesives. Samples were mechanically tested in Mode I, Mode II, and shear. A numerical model was defined in Abaqus 2020 to closely resemble each experimental condition. Data from experimental tests were used to calibrate the numerical model by a novel semi-automatic procedure and compared with numerical outcomes.

The procedure was successful in generating a material card that correlates with the experimental curves.

Materials and Methods

Materials. The adherends for all specimens were obtained from a commercial Mitsubishi STR120N131 provided by Mitsubishi Chemicals (Mitsubishi Chemicals Carbon Fiber and Composites GMBH). This material is a fast-curing sheet-molding compound (SMC) made with a vinyl ester resin reinforced with a 53% weight fraction of TR50S-15L Pyrofil® chopped strands. Whereas tow width, thickness, and length are subject to variation due to the manufacturing process, average values are 8 mm, 0.115 mm, and 25 mm, respectively. The material was extracted from cold storage and cut into preforms of 300 x 300 mm. Preforms were stacked to obtain the desired charge thickness. The charge was compression molded into a specifically designed mold featuring a cavity of 300 x 300 mm into a 15 t down stroke Cannon press. An overview of the equipment used is given in Fig. 1. Plates were extracted from the mold, cooled at room temperature in free air condition, and visually checked for imperfections.

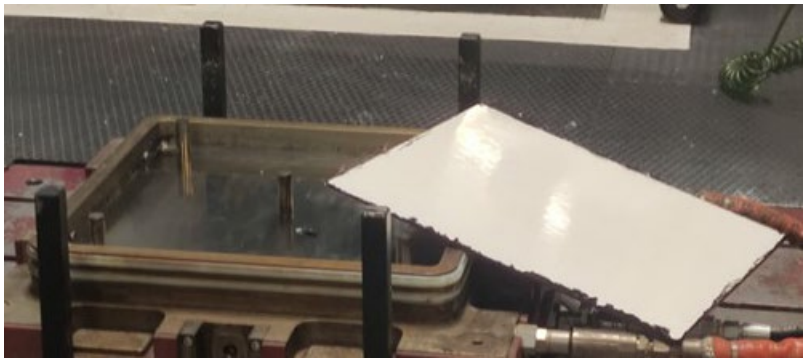

Figure 1 – Designed mold for producing SMC plates in C.P.C. srl

The average value of plate thickness was 4.8 ±0.2 mm. To obtain the desired shapes and sizes of the adherends, plates were cut using a water jet machine. To eliminate any residue of the release agent, adherends were sandblasted and polished with isopropyl alcohol. Adherends were therefore conditioned into a climate chamber at a temperature of 20°C and 30% RH. The adhesive selected was LORD® 7545 Urethane Adhesive (Parker Lord Engineered Materials Group, Cary, USA). LORD® 7545 adhesive is an equal-mix, two-component urethane adhesive system used to bond Fiber Reinforced Plastics (FRP), SMC as well as other plastics with little surface preparation. This adhesive system is capable of being used in a range of working times to accommodate a wide variety of process requirements. According to industrial experience, this adhesive exhibit optimal

performance after a curing period of 7 days at room temperature, during which it achieves a robust bond with excellent mechanical strength.

Sample Preparation. Custom design gluing jigs depicted in Fig. 2 were used to position the adherends. The adhesive was carefully applied by hand using an air gun. The jig was then closed and maintained in a climate chamber at a temperature of 20°C and 30% RH for 7 days to allow a complete crosslink of the adhesive.

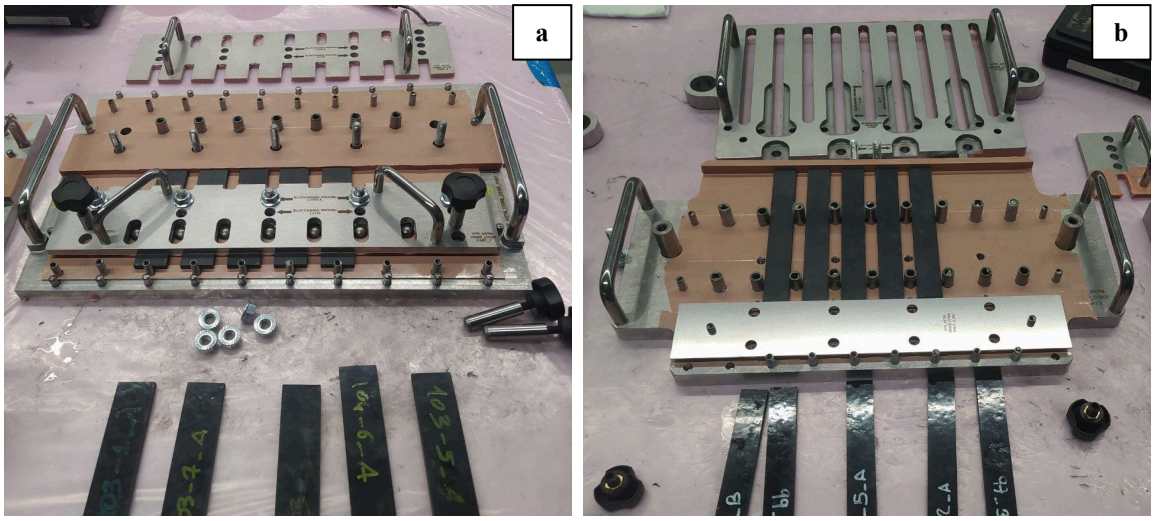

Figure 2 – Custom design gluing jigs: a) SLJ gluing jig, b) DCB and ENF gluing jig

Mechanical Testing. Double Cantilever Beam (DCB), End-Notch Flexure (ENF), and Single-Lap Joinjt (SLJ) test specimens were mechanically tested following ASTM 5528 [14], ASTM 7905 [15], and ASTM 3165 [16], respectively, into an Instron universal testing machine operated in displacement control. Mode I fracture toughness G_{Ic} (J/m^2) of DCB specimens was calculated through the formula:

Where P_{c} (N) is the critical force at break point, δ_{c} (mm) is the relative critical displacement at break point, b (mm) is the width of the specimen and a (mm) is the crack length. Mode II fracture toughness G_{IIc} (J/m^2) was calculated using Eqs. 1 and 2:

$$G_{\mathrm{Ic}} = \frac{3\,P_{\mathrm{c}}\,\delta_{\mathrm{c}}}{2\,b\,a} \cdot 1000 \tag{1}$$

$$G_{\mathrm{IIc}} = \frac{3\,m\,P_{\mathrm{max}}^2\,a_{\mathrm{c}}^2}{2\,b} \cdot 1000 \tag{2}$$

where P_{max} is the maximum force recorded on the force-displacement curve, m (1/Nmm^2) the slope of the linear fit of compliance versus crack length cubed data and b is the specimen width. The crack length a_{c} (mm) was computed through Eq. 3:

$$a_{\mathrm{c}} = \left(\frac{C_{\mathrm{u}} - A}{m}\right)^{1/3} \tag{3}$$

where C_{u} (mm/N) is the specimen compliance after unloading, and A (mm/N) is the intercept of the linear fit of compliance versus crack length cubed data. Single lap joints were evaluated based

Materials Research Proceedings 54 (2025) 478-486 https://doi.org/10.21741/9781644903599-52

on ASTM standards so considering the maximum load at break and the relative shear stress calculated as follows (Eq. 4):

$$\boldsymbol{\tau_{max}} = \frac{\boldsymbol{F_{max}}}{\boldsymbol{A}} \tag{4}$$

Semiautomatic Material Card Generation. A procedure based on the Design of the Experiment (DOE) was adopted to automatically optimize the material card parameters for cohesive zone modeling (CZM) within the commercial code Hyperstudy 2021. Cohesive properties such as elastic moduli, nominal stress of the interface, and fracture energies were considered as design variables and parameterized for variation during the optimization. Targets such as peak force, and critical displacement were extracted from experimental data and defined as objectives within DOE optimization. Constraints were imposed on cohesive material parameters based on industrial experience. The LatinHypercube [17] algorithm was selected to sample the design space by dividing each design variable parameter range into equal intervals and ensuring that each interval is sampled exactly once. Among available alternatives, this method was selected due to its ability to provide a well-distributed representation of the parameter space, allowing for effective exploration and analysis of variable interactions with a relatively small number of simulation runs [18,19]. Results from DOE-generated data were used to create a quadratic response surface, which serves as an approximate model to relate the design variables (elastic moduli, nominal stress of the interface, and fracture energies) to the simulated response of the joint behavior (peak force, and critical displacement). The Global Response Search Method (GRSM) [20] was selected to find the optimal solution. It combines global and local search techniques to optimize complex systems, it reads the response surface using the simulation data and iteratively refines it, and then locates the optimal solution [21]. This process of using DOE, Fitting, and Optimization algorithms is first executed for the DCB specimen, the resulting parameters for Mode I (K_{n},$\mathrm{t}_{\mathrm{n}}^{0}$,$\mathrm{G}_{\mathrm{IC}}$) were then fixed, and the entire process was repeated for the SLJ specimen, finally identifying the remaining properties in Mode II (K_{s},$\mathrm{t}_{\mathrm{s}}^{0}$,$\mathrm{G}_{\mathrm{IIC}}$) and taking Mode III as equal to Mode II. The optimized material card was validated by running test simulations and trying different algorithms, ensuring consistency with experimental observations and algorithm choice.

Numerical Model. The numerical simulations were performed using Abaqus 2020 explicit solver. Each test (DCB, ENF, and SLJ) was simulated closely resembling experimental conditions, including boundary conditions, loading rates, and constraints. Continuum shell elements (S4R) with reduced integration were used to simulate the adherends whilst cohesive elements (COH3D8) were used to simulate the behavior of the adhesive. A 5 mm mesh was adopted to mesh the adherends, whilst a 2.5 mm mesh was used to discretize the adhesive layer following established industrial procedures. Overall, the DCB model accounted for 1071 nodes, the ENF model accounted for 5726 nodes, and the SLJ accounted for 426 nodes (see Fig. 3). As illustrated in Fig. 3a, hinges for DCB were modeled using kinematic coupling, while loading and support surfaces were modeled using rigid body elements (R3D4), as illustrated in Fig. 3b. Within Abaqus, the elastic behavior of the cohesive elements' material is modeled through the relationship (Eq. 5) [22]:

$$\boldsymbol{t} = \begin{Bmatrix} t_{\mathrm{n}} \\ t_{\mathrm{s}} \\ t_{\mathrm{t}} \end{Bmatrix} = \begin{pmatrix} K_{\mathrm{n}} & 0 & 0 \\ 0 & K_{\mathrm{s}} & 0 \\ 0 & 0 & K_{\mathrm{t}} \end{pmatrix} \begin{Bmatrix} \delta_{\mathrm{n}} \\ \delta_{\mathrm{s}} \\ \delta_{\mathrm{t}} \end{Bmatrix} \tag{5}$$

Being $\boldsymbol{t}$ the nominal traction stress vector representing the stress induced by the three deformation modes: the deformation in the normal direction δ_{n} and two shear deformation modes δ_{s} and δ_{t}. The quadratic failure criterion and the Benzeggagh–Kenane (BK) law [23] are employed

to predict the initiation and propagation of delamination damage, expressed in Eqs. (6) and (7) respectively:

$$\left\{\frac{\langle t_n \rangle}{t_n^0}\right\}^2 + \left\{\frac{t_s}{t_s^0}\right\}^2 + \left\{\frac{t_t}{t_t^0}\right\}^2 = 1 \quad (6)$$

where t_n^0, t_s^0, t_t^0 are the peak values of the nominal stress of the interface when separation is merely aligned with the respective fracture mode.

$$G_C = G_{IC} + (G_{IIC} - G_{IC})\left(\frac{G_{II} + G_{III}}{G_I + G_{II} + G_{III}}\right)^{\eta} \quad (7)$$

Being G_C, G_{IC} and G_{IIC} respectively the total, normal and shear critical energies release rates and G_I, G_{II} and G_{III} the energy release rate under Mode I, Mode II, and Mode III respectively. η is the relevant material parameter in the BK law, as well as peak stresses and the critical energy release rates.

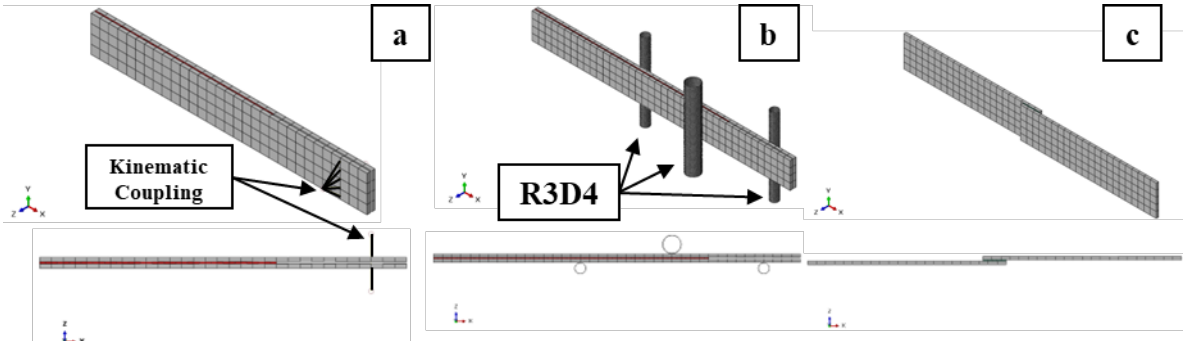

Figure 3 – a) DCB, b) ENF and c) SLJ test specimens mesh models

Results and Discussions

Mechanical Testing. Force vs displacement curves for DCB, ENF, and SLJ specimens are illustrated in Fig. 4a, Fig. 4b, and Fig. 4c, respectively. The curves from the DCB test shared a comparable stiffness up to failure that occurred at different loads between the samples, suggesting inconsistency in crack initiation and propagation. Specimens D1, D2, and D4 exhibited marked load drop after the first failure, while specimens D3 and D5 showed a more gradual stiffness degradation. The ENF test curves, shown in Fig. 4b, display uniformity, with all specimens following a similar linear trend until approximately 3000 N and reaching their maximum load within a narrow range. The observed failure mode invalidated the tests: in all specimens, the failure occurred in the lower adherend rather than the adhesive layer. SLJ test curves (Fig. 4c) also exhibit consistent linear stiffness during the elastic phase, followed by a smoother non-linear region where the force-displacement relationship deviates from linearity. Indeed, at higher forces, the adhesive layer undergoes plastic deformation. This phase transitions to a break point characterized by a

sharp force drop. All specimens failed at a comparable ultimate load except for specimen S4, which failed at 5250 N.

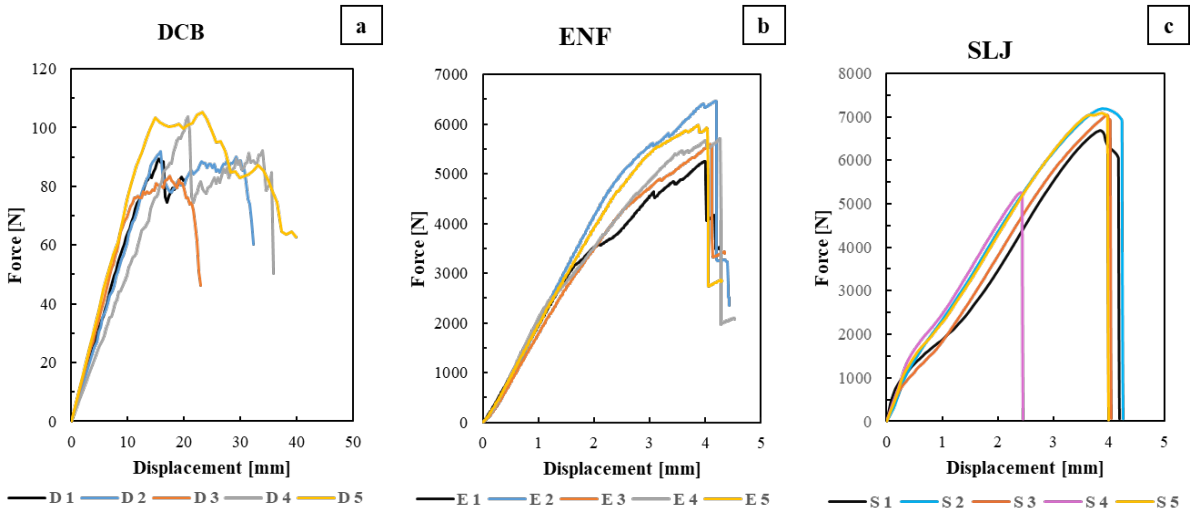

Figure 4 – Load Displacement curves for a) DCB test, b) ENF test and c) SLJ test

Numerical Simulation. The optimization process culminated in what the solver calls an optimal solution: a set of parameters that represents the material card, reported in Table 1.

Table 1 – Optimized parameter set for the Material Card

Material property	Value	Units
K_n	112.90	MPa/mm
$K_s = K_t$	4.38	MPa/mm
t_n^0	3103.50	MPa
$t_s^0 = t_t^0$	452.90	MPa
G_{IC}	56.95	N/mm
G_{IIC}=G_{IIIC}	56.95	N/mm
η	1	-

A comparison between simulative and experimental results is given in Fig. 5. By focusing solely on damage initiation and excluding propagation, it can be observed that the DCB curves exhibit a similar initial linear trend and stiffness. Near the point of failure or maximum force, the generated curve demonstrates a slight increase in stiffness (Fig. 5a), followed by an abrupt load drop followed by crack propagation. The failure predicted by FEA occurs at a force value that is lower than that observed in the experimental results. Consequently, it can be concluded that the data generated by FEA is conservative when compared to the empirical findings. The SLJ curves (Fig. 5b) exhibit notable differences. The experimental curve is influenced by complex physical effects, resulting in a softer appearance. In contrast, the generated curve is more rigid and linear. Both curves exhibit a convergence at a remarkably narrow range of ultimate load capacity, with the numerical one being more conservative in predicting the ultimate load of the joint.

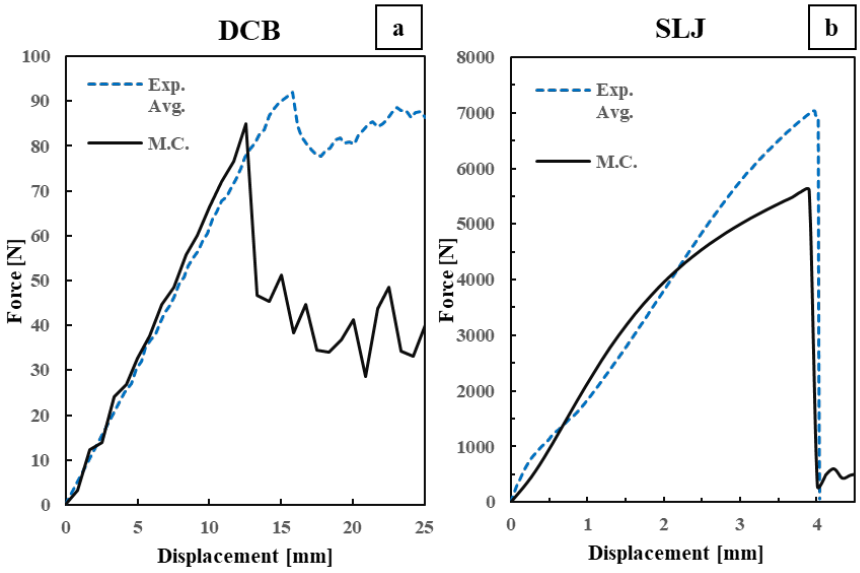

Figure 5 – Comparison between Experimental and numerical Load Displacement curves a) DCB test, b) SLJ test.

Conclusions

In this work, the possibility of investigating the strength of adhesively bonded SMC components by means of numerical tools was successfully demonstrated. The experimental testing phase revealed consistent initial stiffness across all test types (DCB, ENF, and SLJ), with variations primarily occurring at first failure. DCB and SLJ tests provided valuable insights into adhesive and adherend interactions, while the ENF test was demonstrated to be ineffective in characterizing the Mode II fracture toughness of the joint due to consistent failure in the lower adherend. The numerical simulation and optimization process successfully produced a material card that closely replicated experimental force-displacement curves, particularly in terms of stiffness and failure points. Although the simulated DCB curves demonstrated conservative predictions compared to experimental results, and SLJ curves exhibited differences in linear regions due to complex physical effects, the overall agreement at critical points validated the methodology. Future studies will investigate the scalability of the findings to more complex parts and loading scenarios.

Funding

This work was supported by Emilia-Romagna region: “Bando in attuazione dell’art. 6 LR 14/2014 - anno 2022 - accordi regionali di insediamento e sviluppo delle imprese (ARIS)” – Titolo del progetto: “Mobilità del futuro: nuove tecnologie e nuovi materiali per una maggiore sostenibilità. L.R. 14/2014 – DGR 2332/2022; CUP E99J22006860009.” Luca Raimondi and Lorenzo Donati acknowledges the support of Ecosystem for Sustainable Transition in Emilia-Romagna Project, funded under the National Recovery and Resilience Plan (NRRP), Mission 04 Component 2 Investment 1.5—NextGenerationEU, call for tender n. 3277 dated 30 December 2021 Award Number: 0001052 dated 23 June 2022 CUP: B33D21019790006.

References

[1] Troiani E, Falaschetti MP, Taddia S, Ceruti A. CFRP Crash Absorbers in Small UAV: Design and Optimization. SAE Tech. Pap., vol. 2015–Septe, SAE International; 2015. https://doi.org/10.4271/2015-01-2461

[2] Cocchi D, Raimondi L, Brugo TM, Zucchelli A. A systematic material-oriented design approach for lightweight components and the CFRP motor wheel case study. Int J Adv Manuf Technol 2020;109:2133–53. https://doi.org/10.1007/s00170-020-05756-2

[3] Falaschetti MP, Birnie Hernández J, Semprucci F, Raimondi L, Serradimigni D, Troiani E, et al. Analysis of the Crushing Behavior of Flat Composite Plates Produced by Sheet Molding Compound. Dyn. Response Fail. Compos. Mater., Springer; 2025, p. 40–8. https://doi.org/10.1007/978-3-031-77697-7_6

[4] Staff, Gardiner G. Is the BMW 7 Series the future of autocomposites? CompositesWorld 2016.

[5] Ebrahimian F, Rodriguez S, Di Lorenzo D, Chinesta F. Optimization of precharge placement in sheet molding compound process. Int J Mater Form 2024;17. https://doi.org/10.1007/s12289-024-01836-w

[6] Galińska A. Mechanical joining of fibre reinforced polymer composites to metals—a review. Part i: Bolted joining. Polymers (Basel) 2020;12:1–48. https://doi.org/10.3390/polym12102252

[7] Raimondi L, Tomesani L, Zucchelli A. Enhancing the Robustness of Hybrid Metal-Composite Connections Through 3D Printed Micro Penetrative Anchors. Appl Compos Mater 2024. https://doi.org/10.1007/s10443-024-10224-1

[8] Raimondi L, Tomesani L, Donati L, Zucchelli A. Lattice material infiltration for hybrid metal-composite joints: Manufacturing and static strenght. Compos Struct 2021;269:114069. https://doi.org/10.1016/j.compstruct.2021.114069

[9] Cole RT, Bateh EJ, Potter J. Fasteners for composite structures. Composites 1982;13:233–40. https://doi.org/10.1016/0010-4361(82)90005-2

[10] Lopes VHP, Campilho RDSG, Nóvoa PJRO, Rocha RJB, Sánchez-Arce IJ. Experimental and cohesive zone modelling study on composite joining by co-curing and adhesive bonding for sheet moulding compound or carbon-fibre prepreg laminates. J Adhes Sci Technol 2023;37:1593–613. https://doi.org/10.1080/01694243.2022.2081446

[11] Jyoti A, Gibson RF, Newaz GM. Experimental studies of Mode I energy release rate in adhesively bonded width tapered composite DCB specimens. Compos Sci Technol 2005;65:9–18. https://doi.org/10.1016/j.compscitech.2004.04.006

[12] Campilho RDSG, Banea MD, Pinto AMG, Da Silva LFM, De Jesus AMP. Strength prediction of single- and double-lap joints by standard and extended finite element modelling. Int J Adhes Adhes 2011;31:363–72. https://doi.org/10.1016/j.ijadhadh.2010.09.008

[13] Faneco TMS, Campilho RDSG, Silva FJG, Lopes RM. Strength and fracture characterization of a novel polyurethane adhesive for the automotive industry. J Test Eval 2017;45:398–407. https://doi.org/10.1520/JTE20150335

[14] International A. ASTM D5528-01(07). Stand Test Method Mode I Interlaminar Fract Toughness Unicirectional Fiber-Reinforced Polym Matrix Compos 2007;D 5528-0:12.

[15] ASTM. D 7905 Standard Test Method for Determination of the Mode II Interlaminar Fracture Toughness of Unidirectional Fiber-Reinforced Polymer Matrix Composites. ASTM Stand 2012;i:1–16.

[16] ASTM. D3165 Standard Test Method for Strength Properties of Adhesives in Shear by Tension Loading of Single-Lap-Joint Laminated Assemblies 1 2012;2:1–4. https://doi.org/10.1520/D3165-07R14.2

[17] Olsson AMJ, Sandberg GE. Latin Hypercube Sampling for Stochastic Finite Element Analysis. J Eng Mech 2002;128:121–5. https://doi.org/10.1061/(asce)0733-9399(2002)128:1(121)

[18] Gu Z, Liu Y, Hughes DJ, Ye J, Hou X. A parametric study of adhesive bonded joints with composite material using black-box and grey-box machine learning methods: Deep neuron networks and genetic programming. Compos Part B Eng 2021;217. https://doi.org/10.1016/j.compositesb.2021.108894

[19] Liu Y, Gu Z, Hughes DJ, Ye J, Hou X. Understanding mixed mode ratio of adhesively bonded joints using genetic programming (GP). Compos Struct 2021;258:113389. https://doi.org/10.1016/j.compstruct.2020.113389

[20] Mandolfino C, Cassettari L, Pizzorni M, Saccaro S, Lertora E. A Response Surface Methodology Approach to Improve Adhesive Bonding of Pulsed Laser Treated CFRP Composites. Polymers (Basel) 2023;15. https://doi.org/10.3390/polym15010121

[21] Mandolfino C, Cassettari L, Lertora E, Pizzorni M. Adhesive bonding of glass-fibre thermoplastic composite: process optimisation and sustainability analysis using LCA methodology. Int J Adv Manuf Technol 2024;130:5709–26. https://doi.org/10.1007/s00170-024-13022-y

[22] Raimondi L, Bernardi F. Advanced hybrid laminates : elastomer integration for optimized mechanical properties. Int J Adv Manuf Technol 2025:3177–95. https://doi.org/10.1007/s00170-025-15023-x

[23] Benzeggagh ML, Kenane M. Measurement of mixed-mode delamination fracture toughness of unidirectional glass/epoxy composites with mixed-mode bending apparatus. Compos Sci Technol 1996;56:439–49. https://doi.org/10.1016/0266-3538(96)00005-X